VEGAS: A Monte Carlo Simulation of Intranuclear Cascades*

K. CHEN, Z. FRAENKEL,† G. FRIEDLANDER, J. R. GROVER, J. M. MILLER, AND Y. SHIMAMOTO
Brookhaven National Laboratory, Upton, New York
and
Columbia University, New York, New York

(Received 16 August 1967)

The model dependence of the Monte Carlo simulation of intranuclear cascades generated by nucleons up to ~380 MeV incident on complex nuclei has been investigated. Differences in the details of the Monte Carlo procedure between this work and previous intranuclear-cascade calculations are discussed. The specific effects that were investigated are those attendant upon the introduction of refraction of cascade particles when going through regions of varying potential energy, and upon the change in the nuclear density distribution from that of a uniform-density sphere to one with a diffuse surface similar to that consistent with electron-scattering experiments. Among the calculated quantities discussed are reaction cross sections, excitation energies of cascade products, spallation cross sections, energy and angular distributions of emitted particles, and linear and angular momentum transfers. The introduction of the diffuse-surface-density distribution improves agreement with available experimental data. At incident energies below ~200 MeV and for medium and heavy nuclei, best agreement with experimental data is obtained when refraction and reflection are neglected. Possible reasons for this result are discussed.

I. INTRODUCTION

IT has often proved convenient to approximate the interaction of high-energy (>100 MeV) nucleons with complex nuclei as a sequence of two-body interactions between the incident particles and individual nucleons in the nucleus.[1] In the spirit of this approximation, the interactions of the struck nucleons with the remaining target nucleons have then also been considered as a sequence of two-body interactions, the entire initial interaction thus being treated as an intranuclear cascade of fast nucleons which can be calculated in detail. The properties of such calculated cascades were first investigated by Goldberger[2] through the use of the Monte Carlo technique and a two-dimensional model of the nucleus, with the assumption that the characteristics of the nucleon-nucleon collision within nuclear matter are the same as those in free space except for the effect of the Pauli exclusion principle. Several similar investigations of this problem followed; the most detailed of these were the ones of Metropolis *et al.*[3] and of Bertini.[4] Both of these were carried out with electronic computers, included a large number of events, and used a three-dimensional model. Other such calculations have been reported from the Los Alamos[5] and Orsay laboratories.[6]

While the results of the calculation by Metropolis *et al.* show good agreement with some experimental results, that calculation contains two approximations (partly dictated by computer limitations) which are at least dubious and the effects of which should be investigated. These are (a) the use of a uniform-density nucleus with a sharp boundary and (b) the neglect of the refraction and reflection of cascade nucleons due to spatial nonuniformity of the nuclear potential. The advent of fast computers with larger fast memories than were previously available makes practicable the use of less drastic approximations, and in the recent calculations by Bertini[4] the effects of changing from a uniform to a nonuniform radial density distribution were investigated.

The principal features in the calculations reported here are (a) the use of nuclear density and potential-energy distributions with diffuse boundaries, (b) the inclusion of refraction and thus possible reflections of nucleons at the nuclear surface and at assumed boundaries between regions of different potential energy, (c) an attempt to follow the spatial and temporal development of each cascade, (d) investigations of the effects of various model assumptions and parameter choices. This paper is concerned only with the energy range in which pion production and subsequent interactions are unimportant ($\lesssim$380 MeV). Our calculation, which we have called VEGAS, was carried out using an IBM 7094 computer. FORTRAN 66 programs of VEGAS are available for use with the CDC 6600 also.

In this calculation the history of each cascade particle is stored on magnetic tape. The following information is recorded; the cascade number; the identity of the particle (proton or neutron); whether or not it left the nucleus, its mass, momentum, and energy; its final position (in x, y, z coordinates) and corresponding direction cosines; and the time and position of each of its interactions with other particles. Various editing routines may be used to derive, from the data available on tape for a given set of cascades, such information as:

* Research performed under the auspices of the U. S. Atomic Energy Commission.

† Permanent address: Weizmann Institute of Science, Rehovoth, Israel.

[1] R. Serber, Phys. Rev. **72**, 1114 (1947).
[2] M. L. Goldberger, Phys. Rev. **74**, 1269 (1948).
[3] N. Metropolis, R. Bivins, M. Storm, A. Turkevich, J. M. Miller, and G. Friedlander, Phys. Rev. **110**, 185 (1958); **110**, 204 (1958).
[4] H. W. Bertini, Phys. Rev. **131**, 1801 (1963).
[5] R. L. Bivins, D. R. F. Cochran, S. L. Whetstone, and J. K. Wooten, Los Alamos Report No. LA-3206-MS (unpublished).
[6] E. Gradsztajn, Ann. Phys. (Paris) **10**, 791 (1965); J. P. Cohen, Nucl. Phys. **84**, 316 (1966).

energy and angular distributions of outgoing particles; mass, charge, excitation energy, momentum, and angular momentum of residual nuclei; and correlations between these quantities.

In Sec. II we describe the nuclear models that were investigated. In Sec. III the program of the calculations is discussed insofar as it differs from other published calculations. Section IV is devoted to comparisons of some of the results of calculations made with the different nuclear models described in Sec. II and to comparisons with experimental data. Some conclusions from these comparisons are discussed in Sec. V.

II. NUCLEAR MODELS

Three alternative models for the nuclear density distribution were considered: (a) a constant-density nucleus of radius $r=r_0A^{1/3}$ with $r_0=1.3\times10^{-13}$ cm (the model used by Metropolis *et al.*[3]); (b) a trapezoidal density distribution

$$\begin{aligned}\rho(r)&=\rho_0 && \text{if} \quad r\leqslant c-\tfrac{1}{2}\Delta,\\ &=\rho_0(c+\tfrac{1}{2}\Delta-r)/\Delta && \text{if} \quad c-\tfrac{1}{2}\Delta<r\leqslant c+\tfrac{1}{2}\Delta,\\ &=0 && \text{if} \quad r>c+\tfrac{1}{2}\Delta,\end{aligned} \tag{1}$$

where c, the radius at which the density has fallen off to $\frac{1}{2}$ the density at the center of the nucleus, is given by

$$c=r_0A^{1/3} \quad r_0=1.07\times10^{-13} \text{ cm}$$

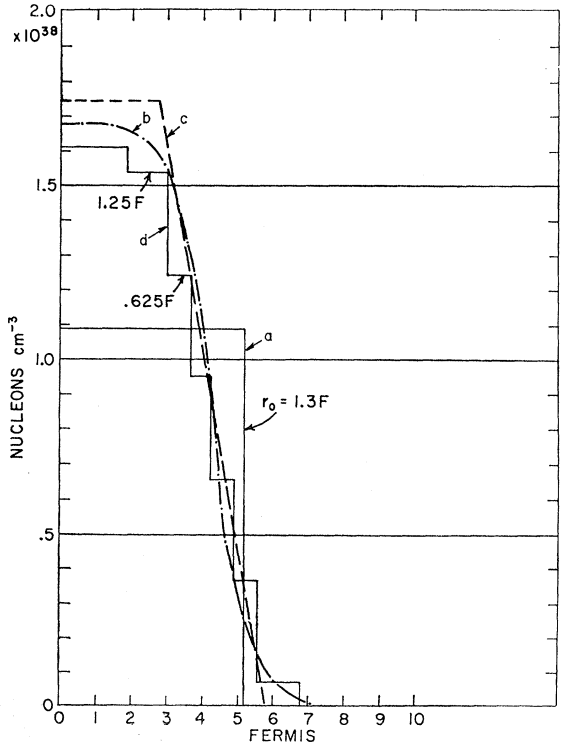

FIG. 1. Four models of nuclear density distribution for Cu^{64}. (a) Uniform density used in Ref. 3; (b) Fermi distribution of Ref. 7; (c) trapezoidal distribution of Eq. (1); (d) step-function distribution described in text.

and the "skin thickness" was chosen as

$$\Delta=3\times10^{-13} \text{ cm};$$

(c) a step-function density distribution which is depicted in Fig. 1 and described below in detail.

The momentum distribution of the nucleons in the nucleus was assumed to be that of a degenerate Fermi gas with the Fermi energy given by

$$E_{F_i}=(\hbar^2/2m)(3\pi^2\rho_i)^{2/3}, \tag{2}$$

where the subscript i stands for either protons or neutrons, m is the nucleon mass, and ρ_i is the density of protons and neutrons, respectively. In the models with trapezoidal and step-function density distributions, the Fermi energy at any point in the nucleus was computed from the corresponding density. The negative of the potential energy at any given point was taken as the Fermi energy plus the average of the binding energies of the most loosely bound neutron and proton.

The nuclear charge distribution as measured by Hofstadter[7] may be represented either by the trapezoidal distribution of Eq. (1) or by the Fermi distribution

$$\rho(r)=\rho_0/[1+\exp(r-c)/a], \tag{3}$$

with $c=1.07A^{1/3}\times10^{-13}$ cm and

$$t=r_{0.1}-r_{0.9}=4.4a=2.4\times10^{-13} \text{ cm},$$

where $r_{0.1}$ and $r_{0.9}$ are the radii at which the density has dropped to $0.1\rho_0$ and $0.9\rho_0$, respectively. Assuming the shape of the nuclear-density distribution to be identical with the shape of the measured charge distribution, we see that the trapezoidal distribution of Eq. (1) is not very different from the Fermi distribution for

$$r<r_{0.1}=c+\tfrac{2}{5}\Delta.$$

The trapezoidal distribution was our first attempt to take into account the effect of the diffuse edge of the nucleus. It has, however, two disadvantages: (i) It does not leave any freedom to vary the manner in which the density approaches zero since the slope is fixed by the electron scattering data; (ii) if refraction due to changes in nuclear density is taken into account in the calculation (see below), continuously changing densities cause time-consuming computational difficulties. As to the first objection, a good representation of the very diffuse outer edge of the nucleus may at first not seem to be of great importance in high-energy nuclear reactions. However, this is not so. It is this portion of the nucleus that is largely responsible for the relatively high yield of very short nuclear cascades such as (P,P), (P,N), (P,PN), $(P,2P)$.[8] These cascades are mainly produced when the incoming particle strikes the nucleus at a large impact parameter and does not

[7] R. Hofstadter, Ann. Rev. Nucl. Sci. **7**, 295 (1957).

[8] J. R. Grover and A. A. Caretto, Jr., Ann. Rev. Nucl. Sci. **14**, 51 (1964).

enter the denser regions of the nucleus. If it does make an interaction in this very diffuse outer edge of the nucleus, the probability of both interaction partners escaping from the nucleus without further interaction is relatively high.

As a consequence, neither the constant-density model nor the trapezoidal model were extensively used in the calculations to be reported here. The constant-density model was used primarily in order to compare the results of our calculations with previous calculations which used this model, in particular the work of Metropolis *et al.*[3] In most of our calculations, a step-function distribution (Fig. 1) was used to approximate the Fermi distribution [Eq. (3)] by seven concentric regions, each of constant density. The outer radius of the central region is $c-2.50$ F (with $c=1.07A^{1/3}$ F), while the radius of the nucleus is taken to be $c+2.50$ F. The outermost region is taken to be 1.25 F thick, the next four regions are each 0.625 F thick, and the first step from the top is again 1.25 F thick. The density ρ_1 of region 1 (the outermost region) is determined by the condition that it contain the same number of nucleons as the region outside the sphere of radius r_1 in the Fermi distribution where $r_1=c+1.25$ F. The distance r_1 is the inner radius of the region 1 in the step distribution and corresponds to the radius at which the density of the Fermi distribution has fallen to 10% of the maximum value, $\rho(r_1)=0.1\rho_0$. In other words, the same number of nucleons are contained outside the sphere of radius $r_1=(1.07A^{1/3}+1.25)\times10^{-13}$ cm in both distributions. The difference in density between the innermost region (region 7) and the adjoining region (region 6) is again ρ_1, whereas the density differences between all intermediate regions, δ, are equal;

$$\delta=\rho_2-\rho_1=\rho_3-\rho_2=\rho_4-\rho_3=\rho_5-\rho_4=\rho_6-\rho_5.$$

The quantity δ is determined by the condition that the total number of nucleons in the nucleus be A. The momentum distribution of the protons and neutrons in each density region is, as stated before, assumed to be that of a degenerate Fermi gas. The Fermi energy is given by Eq. (1) with ρ_i the proton or neutron density, respectively, for the region in question. The ratio of proton density to neutron density is assumed to be $Z/(A-Z)$ in all regions.

As a consequence of the variation of the Fermi energy, the nuclear potential of the protons and neutrons differs in the various density regions. Conservation of energy requires, therefore, that the kinetic energy of the particles must also change as they cross from one density region into the adjoining region. All previous calculations of the intranuclear-cascade process which have taken into account the change in the kinetic energy as a result of changing nuclear potential have done so by changing the kinetic energy of the cascade particle without changing its direction of motion. In the present paper we discuss and compare the results of calculations both with and without the change in direction required by the changing nuclear potential, that is, with and without the refraction and reflection appropriate to a central potential.

To calculate the refraction of a particle, the radial component of the particle momentum is changed as the particle enters a different density region, while the tangential component is unchanged. Thus, assuming the usual invariance of E^2-p^2, we have

$$p_R'^2=p_R^2+E'^2-E^2, \tag{4}$$

where p_R is the radial component of the momentum of the particle, E is its total energy, and the primed and unprimed values correspond to the new and old density regions, respectively, and where the units are such that $c=1$.

The new energy E' is given by

$$E'=E-(V'-V), \tag{5}$$

where V and V' are the values of the nuclear potential in the old and new regions. To conserve the tangential component of momentum, the angle of refraction is given by

$$\frac{\sin\theta}{\sin\theta'}=\frac{p'}{p}. \tag{6}$$

The critical angle for total reflection θ_{cr} comes from Eqs. (4) and (6) under the condition that $\sin\theta'=1$:

$$\cos\theta_{cr}=(E^2-E'^2)^{1/2}/p. \tag{7}$$

The cascade particles are followed until their total energy (kinetic plus potential plus mass) drops below some cutoff energy. The cutoff energy is treated as a free input parameter and it may have different values for protons and for neutrons. The cutoff energies in the calculation reported here are as follows: (a) for cascade neutrons, the Fermi energy plus twice the average binding energy; (b) for cascade protons, either the Fermi energy plus twice the average binding energy or the Fermi energy plus the sum of the average binding energy and the Coulomb barrier, whichever is the larger. A single average value is used for the binding energies of both protons and neutrons for a given starting nucleus (obtained from mass tables as the average of the binding energies of the last few nucleons in this nucleus), and the same value is used throughout the calculation (i.e., independently of how many nucleons have escaped from the nucleus). The Fermi energies for the residual nucleons are not changed as nucleons leave the nucleus. Hence the nuclear potential is assumed not to change during the cascade stage of the high-energy nuclear reaction.

Both the residual excitation and the recoil momentum of the nucleus at the end of the cascade stage are recorded as part of the output data. The residual excitation energy is calculated as in Metropolis *et al.*[3] and the recoil momentum is obtained by subtracting the mo-

mentum of all outgoing particles from the momentum of the bombarding particle. The residual angular momentum of the nucleus may be calculated in an analogous way.

The effect of the Coulombic interaction between the target nucleus and incident and emitted charged particles is explicitly considered in this calculation in only one way: The refraction of cascade protons crossing the nuclear boundary is appropriate to a potential energy just outside the nuclear boundary which is the Coulomb potential rather than zero potential as for neutrons. The Coulomb deflection of protons outside of the region of nuclear potential need not be considered explicitly in the Monte Carlo program because this deflection has no effect upon the form of the distribution of impact parameters of the incident particle. Other than the energy and the identity of the incident particle, the impact parameter is the only quantity of significance to a cascade, since the internal properties of a calculated cascade are independent of any rotations of the coordinate system. This remark is, of course, not true for external properties of the cascade such as the direction cosines of the emitted particles and therefore also the recoil properties of product nuclei.

That the Coulomb deflection does not change the distribution of impact parameters may be seen from two relations;

$$b'=b(1-B/\mathcal{E})^{-1/2}, \tag{8}$$

$$W(b)db=2\pi bdb/\pi R^2, \tag{9}$$

where b and b' are the impact parameters of an incident particle at infinity and at the surface of the nucleus after Coulomb deflection, respectively, $\mathcal{E}$ is the kinetic energy of the incident particle at infinity, B is the electrostatic potential energy of the system when the incident particle is at the surface of the nucleus, and $W(b)$ is the probability density for an impact parameter b at infinity. Equation (8) comes directly from the conservation of angular momentum assuming that there is not yet any excitation of the target nucleus by the incident particle. From Eqs. (8) and (9) it follows that

$$W'(b')db'=[(1-B/\mathcal{E})/\pi R^2]2\pi b'db', \tag{10}$$

which shows that the probability of a given impact parameter at the nuclear surface after Coulomb deflection is still proportional to the impact parameter.[9] The additional factor of $(1-B/\mathcal{E})$ merely means that the maximum impact parameter at infinity that can lead to a nuclear reaction is $R(1-B/\mathcal{E})^{1/2}$ instead of R and thus that the reaction cross section can be no larger than $\pi R^2(1-B/\mathcal{E})$. It is the latter quantity which is used when cross sections for various events are estimated from the present calculation.

The correction of "external" properties of the cascades for Coulombic deflection may be effected by the straightforward use of transformation matrices which represent appropriate rotations of the coordinate systems. The appropriate rotations correspond to angular deflections of the incident and each of the emitted particles in the Coulomb field of the nucleus. These corrections were *not* made in the results to be reported here because they are nearly always negligible. For example, if we consider the emission of protons from a uranium nucleus at an impact parameter equal to the radius, where the effect is the largest, the Coulomb deflections of protons of 25, 50, and 100 MeV are, respectively, 22.8°, 6.6°, and less than 1°.

[9] Equation (8) is correct nonrelativistically. Introduction of its relativistic equivalent does not change the conclusion.

III. SOME DETAILS OF THE CALCULATION

Only those aspects of the present calculation that differ significantly from previous similar calculations[3] will be examined in this section.

A. Elementary Interaction Cross Sections

Differential cross sections for the intranuclear nucleon-nucleon collisions were obtained by interpolation of the values given in Tables I and II. These tables give normalized differential cross sections for elastic scattering, together with the corresponding total cross sections for neutron-proton collisions (Table I) and for proton-proton and neutron-neutron collisions (Table II). Linear interpolations for both energy and angle were used with the normalized differential cross section entries. The total cross sections were obtained from the following expressions which approximate the values given in Tables I and II.

For p-n collisions,

$$\sigma=-\frac{5057.4}{E^2}+\frac{9069.2}{E}+6.9466 \text{ mb}, \qquad E\leqslant 40 \text{ MeV}$$

$$\sigma=\frac{239\,380}{E^2}+\frac{1802.0}{E}+27.147 \text{ mb}, \qquad 40<E\leqslant 400 \text{ MeV}$$

$$\sigma=34.5 \text{ mb}, \qquad 400<E\leqslant 800 \text{ MeV};$$

while those for p-p and n-n collisions are

$$\sigma=-\frac{1174.8}{E^2}+\frac{3088.5}{E}+5.3107 \text{ mb}, \qquad E\leqslant 40 \text{ MeV}.$$

$$\sigma=\frac{93074}{E^2}-\frac{11.148}{E}+22.429 \text{ mb}, \qquad 40<E\leqslant 310 \text{ MeV}$$

$$\sigma=\frac{887.37}{E}+0.05331E+3.5475 \text{ mb}, \qquad 310<E\leqslant 800 \text{ MeV}.$$

The quantity E in the above equations is the kinetic energy of one of the particles in the laboratory system incident on the other particle at rest.

TABLE I. Angular distributions, total elastic cross sections, and total interaction cross sections for neutron-proton collisions. Entries for the differential cross sections[a] are values of $(d\sigma_{el}/d\Omega)/\sigma_{el}$, in the c. m. system. The angle $\theta_{c.m.}$ refers to the direction of motion of the neutron.

E_{lab} (MeV)	$E_{c.m.}$ (MeV)	$\cos\theta_{c.m.}=$ 1.00	0.99	0.96	0.90	0.8	0.7	0.6	0.5	0.4	0.3	0.2	0.1	0
≤ 14	≤ 7.0	0.080	0.080	0.080	0.080	0.080	0.080	0.080	0.080	0.080	0.080	0.080	0.080	0.080
25	12.5													
40	19.9	0.099	0.099	0.097	0.095	0.091	0.088	0.085	0.082	0.079	0.075	0.073	0.071	0.071
60	29.7	0.127	0.125	0.120	0.111	0.098	0.088	0.079	0.072	0.068	0.065	0.065	0.064	0.064
90	44.4	0.162	0.154	0.132	0.113	0.096	0.082	0.073	0.067	0.063	0.060	0.057	0.055	0.055
135	66.3	0.183	0.163	0.139	0.121	0.096	0.076	0.062	0.053	0.0490	0.0480	0.0476	0.0478	0.0486
200	97.4	0.260	0.213	0.137	0.104	0.080	0.069	0.062	0.057	0.052	0.0478	0.0445	0.0436	0.0458
300	144.4	0.179	0.160	0.134	0.111	0.099	0.089	0.081	0.073	0.066	0.059	0.054	0.050	0.0488
400	190.2	0.226	0.180	0.148	0.123	0.104	0.091	0.081	0.074	0.068	0.062	0.056	0.052	0.0493
600	279.1	0.426	0.343	0.235	0.179	0.137	0.109	0.089	0.074	0.063	0.055	0.0481	0.0422	0.0378
800	364.4	0.626	0.465	0.317	0.222	0.152	0.116	0.091	0.072	0.061	0.052	0.0447	0.0398	0.0353

TABLE I (*continued*).

E_{lab} (MeV)	$E_{c.m.}$ (MeV)	$\cos\theta_{c.m.}=$ −0.1	−0.2	−0.3	−0.4	−0.5	−0.6	−0.7	−0.8	−0.9	−0.96	−0.99	−1.00	σ_{el} (mb)	σ_{tot} (mb)
≤ 14	≤ 7.0	0.080	0.080	0.080	0.080	0.080	0.080	0.080	0.080	0.080	0.080	0.080	0.080		
25	12.5													381	381
40	19.9	0.071	0.071	0.072	0.073	0.075	0.077	0.079	0.082	0.086	0.090	0.094	0.095	214.5	214.5
60	29.7	0.065	0.067	0.069	0.072	0.075	0.079	0.084	0.090	0.101	0.107	0.112	0.113	130.0	130.0
90	44.4	0.057	0.060	0.063	0.068	0.075	0.082	0.092	0.105	0.123	0.141	0.159	0.187	78.0	78.0
135	66.3	0.051	0.055	0.060	0.067	0.074	0.083	0.096	0.120	0.160	0.193	0.216	0.224	53.5	53.5
200	97.4	0.051	0.057	0.064	0.071	0.080	0.090	0.101	0.121	0.151	0.196	0.254	0.279	41.6	41.6
300	144.4	0.0480	0.0494	0.052	0.057	0.063	0.072	0.086	0.108	0.143	0.182	0.234	0.331	35.9	35.9
400	190.2	0.0472	0.0467	0.0482	0.052	0.058	0.068	0.082	0.102	0.134	0.180	0.252	0.389	33.5	34.2
600	279.1	0.0348	0.0331	0.0334	0.0365	0.0430	0.052	0.067	0.089	0.126	0.170	0.235	0.329	25.9	34.3
800	364.4	0.0317	0.0293	0.0284	0.0291	0.0313	0.0407	0.056	0.078	0.109	0.138	0.183	0.268	18.9	34.9

[a] See Refs. 12–19.

The angles in Table I refer to the direction of motion of the neutron. For energies greater than 200 MeV in the c.m. system, in both Tables I and II, the total cross section becomes appreciably larger than the elastic cross section, while the tabulated angular distributions are for elastic scattering only. The angular distributions, adjusted to the total cross sections, were nevertheless used up to 800 MeV because pion production was not taken into account.

The neutron-proton total and differential cross sections used in the calculations were smoothed experimental values as far as possible. In regions where data are scanty or nonexistent, plausible extrapolations or interpolations were made. Hand-smoothing was carried out, first as a function of energy, with angles held constant, then as a function of angle, at constant energy. The proton-proton differential cross sections are similarly smoothed experimental values outside the regions strongly influenced by Coulomb scattering. For calculating intranuclear proton-proton collisions we used only

TABLE II. Angular distribution, total elastic cross sections, and total interaction cross sections for proton-proton and neutron-neutron collisions. Entries for the differential cross sections[a] are values of $2(d\sigma_{el}/d\Omega)/\sigma_{el}$ in the c. m. system.

E_{lab} (MeV)	$E_{c.m.}$ (MeV)	$\cos\theta_{c.m.}=$ 1.00	0.96	0.9	0.8	0.7	0.6	0.4	0.2	0	σ_{el} (mb)	σ_{tot} (mb)
≤20	≤10	0.159	0.159	0.159	0.159	0.159	0.159	0.159	0.159	0.159		
40	19.9	0.201	0.195	0.187	0.176	0.169	0.160	0.146	0.143	0.143	80.6	80.6
60	29.8	0.194	0.184	0.171	0.162	0.160	0.157	0.154	0.154	0.154	48.0	48.0
80	39.6	0.216	0.202	0.187	0.174	0.164	0.156	0.148	0.146	0.145	36.6	36.6
100	49.4	0.246	0.225	0.202	0.179	0.164	0.155	0.144	0.138	0.138	31.6	31.6
170	83.2	0.299	0.255	0.210	0.174	0.157	0.146	0.140	0.140	0.140	25.9	25.9
250	121.1	0.278	0.231	0.186	0.160	0.153	0.150	0.150	0.148	0.148	24.0	24.0
310	149.1	0.221	0.187	0.159	0.155	0.155	0.156	0.156	0.158	0.159	23.1	23.1
350	167.5	0.190	0.168	0.159	0.156	0.156	0.156	0.157	0.162	0.162	23.1	24.0
460	217.4	0.198	0.192	0.171	0.163	0.161	0.158	0.157	0.151	0.147	23.5	28.3
560	261.7	0.368	0.261	0.210	0.182	0.165	0.153	0.139	0.128	0.123	24.9	33.6
660	305.2	0.72	0.318	0.264	0.219	0.184	0.156	0.115	0.091	0.082	25.0	41.5
800	364.6	0.92	0.444	0.363	0.265	0.193	0.143	0.076	0.0475	0.0399	22.3	47

[a] See Refs. 12–19.

the nucleonic part of the scattering cross section. The differential cross sections inside the regions of appreciable Coulomb scattering were estimated as follows. At 560 MeV and larger energies, where effects of Coulomb scattering are confined to very small angles, the differential cross section at and near 0° (180°) could be obtained from plausible extrapolations of the data at larger angles. At 310, 156, and 40 MeV the tabulated scattering amplitudes of Kerman, McManus, and Thaler[10] were used in the angular regions dominated by Coulomb scattering; smooth curves were drawn through the calculated points with respect to both energy and angle, and made to join smoothly also with the experimental data outside the Coulomb scattering region. This still leaves an awkward gap at 0° between 310 and 560 MeV. Here, the optical theorem $\sigma_{\text{tot}}=4\pi\lambda\,\text{Im}f(0)$ was used to obtain a lower limit from the total cross section, since $(d\sigma/d\Omega)(0°)=|f(0)|^2\geqslant[\text{Im}f(0)]^2$. With this safeguard, the gap was simply bridged with a smooth curve that looked plausible with respect to both energy and angle. For angles larger than 10°, no such hiatus occurs. The proton-proton total cross sections were taken from the compilation of Barashenkov and Maltsev,[11] for energies larger than 2 MeV. Values at $\leqslant 2$ MeV were calculated by the method of scattering lengths. The experimental data used for constructing Tables I and II and for the total-cross-section formulas given above were taken from Refs. 12–19.

B. Method Used for Following Cascade Development

An important difference between previous calculations and the present computer program lies in the sequence in which the "history" of the particles taking part in the intranuclear cascade is followed. Previous calculations followed one particle at a time from its first interaction with another cascade particle (or its entrance into the nucleus in case of the incoming particle) until either its energy fell below the cutoff energy or it escaped from the nucleus. First the incoming particle was so followed, then each of the particles with which the incoming particle had interacted, and in this manner the trajectories of all the other cascade particles were calculated one after the other.

In the present calculation the development of the intranuclear cascade is followed on a timelike basis: In a manner discussed in the Appendix, small time intervals τ are chosen, and in each time interval the progress of all cascade particles above the cutoff energy and inside the nucleus is calculated and recorded. Thus at first only the incoming particle is followed, but after the first allowed interaction both the incoming particle and its collision partner are followed in each time interval, and with each allowed interaction the number of particles to be followed in the subsequent interval increases. The resultant difference, then, from the mechanics of previous calculations is that in the earlier calculations the site of a collision was determined by the correlation between a random number and the partial integration of the probability of the cascade particle to interact at a distance between a and $a+da$ [Eq. (A3)], whereas in the present calculation a random number determines whether the particle makes a collision in each of the many small but finite segments of its path.

The basic results of the Monte Carlo calculation are, of course, independent of the method by which the cascade particles are followed. The advantage of the time-sequence calculation method employed in the present program is that it makes it possible, in principle, to take into account effects of correlation between two close cascade particles and to consider local changes in the nuclear potential and nuclear density due to previous interactions. However, in the calculations to be discussed in this paper, these presumably secondary effects were ignored. The disadvantage of the time-sequence method as compared to the particle-sequence method of previous calculations lies in the greater logical complexity of the computer program.

C. Selection of Collision Partners and Sites

Another phase of the calculation in which the present program differs from previous intranuclear cascade calculations concerns the choice of the interaction partner. The choices of collision partners and collision sites are related and the details of how they were made in these calculations are discussed in the Appendix. The two significant points are that the method outlined in the Appendix is convenient for following the cascade on a timelike basis as discussed in Sec. IIIB, and that the collision partner may be randomly selected directly from the momentum distribution of the target nucleons in the nucleus rather than from that distribution weighted by the relative velocity and by the scattering cross section (relative-velocity dependent) of a pair of colliding nucleons. The latter point introduces great convenience either when the scattering cross section is not a simple function of the relative velocity or when

[10] A. Kerman, H. McManus, and R. Thaler, Ann. Phys. (N. Y.) **8**, 551 (1959).
[11] V. S. Barashenkov and V. M. Maltsev, Fortschr. Physik **9**, 549 (1961).
[12] W. N. Hess, Rev. Mod. Phys. **30**, 368 (1958).
[13] M. D. Goldberg, V. M. May, and J. R. Stehn, Brookhaven National Laboratory Report No. BNL-400, 1962 (unpublished).
[14] J. R. Stehn, M. D. Goldberg, B. A. Magurno, and R. Wiener-Chasman, Brookhaven National Laboratory Report No. BNL-325, 2nd ed., Suppl. No. 2, 1964 (unpublished).
[15] J. P. Scanlon, G. H. Stafford, J. J. Thresher, P. H. Bowen, and A. Langsford, Nucl. Phys. **41**, 401 (1963).
[16] J. L. Gammel, in *Fast Neutron Physics, Part II*, edited by J. B. Marion and J. L. Fowler (Interscience Publishers, Inc., New York, 1963), p. 2185.
[17] J. N. Palmieri, A. M. Cormack, N. F. Ramsey, and R. Wilson, Ann. Phys. (N. Y.) **5**, 299 (1958).
[18] T. Fujii, G. B. Chadwick, G. B. Collins, P. J. Duke, N. C. Hien, M. A. R. Kemp, and F. Turkot, Phys. Rev. **128**, 1836 (1962).
[19] R. Wilson, *The Nucleon-Nucleon Interaction* (Interscience Publishers, Inc., New York, 1963).

the momentum distribution is more complicated than that for a Fermi gas.

IV. COMPARISONS AMONG MODELS AND WITH EXPERIMENTAL DATA

As was described in Sec. II, three different nuclear-density distributions were investigated in the present calculation: uniform, trapezoidal, and step. They are designated as SQUA, TRAP, and STEP, respectively. Further, each of these density distributions was investigated with and without inclusion of the refraction caused by a change in potential energy; these two situations are designated by the addition of no suffix and by the addition of the suffix NO, respectively. For example, SQUA indicates the uniform-density distribution with refraction and STEPNO indicates the step-function density distribution without refraction. Thus, a total of six different models were investigated. As discussed in Sec. II, the STEP model was expected to conform best to the interaction of high-energy nucleons with complex nuclei.

In this section, the results obtained with these six models are compared with each other and with some experimental data. An attempt is made to pinpoint those calculated quantities that are primarily sensitive to the density distribution assumed and those that are strongly affected by the inclusion or neglect of refraction. However, as will be seen, it is not always possible to disentangle these two effects—they often interact with each other in ways that are difficult to rationalize.

A. Reaction Cross Section

The first obvious quantity that should be compared is the reaction cross section predicted by each of the models. Some relevant information is presented in Tables III and IV for the interactions of 378-MeV protons with As^{75} and of 375-MeV protons with Bi^{209} targets, respectively. There it may be seen that the maximum spread in geometrical cross section among the various models is much larger than the maximum spread in reaction cross section. This relative insensitivity of reaction cross section to model is expected because the diffuse edge of the TRAP and STEP models gives rise to increased transparencies. The effect of refraction on reaction cross section is also as expected: The inclusion of refraction will always increase the projected path length of the incident particle through the nucleus and, for the models with diffuse surfaces, will increase the probability that the incident particle will enter a region of greater density. Both of these effects enhance the probability of an interaction by the incident particle and thereby decrease the transparency of the target nucleus.

Comparisons between calculated and measured reaction cross sections are presented in Table V. There it is

TABLE III. Comparison among different models: Interaction of As^{75} with 378-MeV protons.

	σ_{geom} (mb)	σ_{inel} (mb)	$\bar{n}_p$[a]	$\bar{n}_n$[a]	Av. excitation energy $\bar{U}$ (MeV)
SQUA	920	800	1.011	1.045	129.9
SQUANO	920	760	1.603	1.507	74.8
TRAP	1130	818	1.110	1.113	105.4
TRAPNO	1130	735	1.538	1.463	83.4
STEP	1540	907	1.186	1.214	89.9
STEPNO	1540	804	1.443	1.362	70.6

[a] $\bar{n}_p$ and $\bar{n}_n$ are the average numbers of cascade protons and neutrons, respectively, emitted per inelastic cascade.

TABLE IV. Comparison among different models: Interaction of Bi^{209} with 375-MeV protons.

	σ_{geom} (mb)	σ_{inel} (mb)	$\bar{n}_p$[a]	$\bar{n}_n$[a]	Av. excitation energy $\bar{U}$ (MeV)
SQUA	1869	1701	0.666	1.285	175.7
SQUANO	1869	1632	1.146	1.992	110.4
TRAP	1935	1606	0.702	1.340	169.5
TRAPNO	1935	1434	1.129	1.902	126.6
STEP	2460	1725	0.777	1.426	149.6
STEPNO	2460	1556	1.095	1.804	119.2

[a] $\bar{n}_p$ and $\bar{n}_n$ are the average numbers of cascade protons and neutrons, respectively, emitted per inelastic cascade.

TABLE V. Comparison between calculated and experimental inelastic cross sections for proton interactions.

Target nucleus	Incident energy (MeV)	Model	σ_{calc}[a] (mb)	σ_{expt}[b] (mb)
Al^{27}	95	STEP	555±8	
		STEPNO	448±7	415
	160	STEP	475±8	400
Cu^{65}	80	STEP	1036±26	
		STEPNO	790±23	780
	160	STEP	888±25	
		STEPNO	748±23	750
	300	STEP	811±24	
		STEPNO	687±22	635
As^{75}	378	STEP	907±21	
		STEPNO	804±20	
		TRAP	818±17	
		TRAPNO	735±16	~700
		SQUA	800±15	
		SQUANO	760±15	
Ag^{108}	300	STEP	1130±26	~920
Ta^{181}	375	STEP	1564±26	
		STEPNO	1443±25	~1340
Bi^{209}	60	STEP	1883±60	
		STEPNO	1400±52	1680
		SQUANO	1315±42	
	140	STEP	1821±64	
		STEPNO	1480±57	1700
		SQUANO	1504±50	
	375	STEP	1725±34	
		STEPNO	1556±35	
		TRAP	1606±32	
		TRAPNO	1434±30	~1500
		SQUA	1701±32	
		SQUANO	1632±31	
U^{238}	155	STEP	1955±22	~1920

[a] The errors shown are standard deviations.
[b] The experimental cross sections were taken from curves given by A. Johansson, U. Svanberg, and O. Sundberg, Arkiv Fysik **19**, 527 (1961). References to the original sources are given in that paper. "Approximate" signs indicate interpolated values.

seen that the STEP model, over a wide region of energies and target masses, overestimates the magnitude of reaction cross sections and often gives poorer agreement with experimental results than do some of the other models.

B. Average Number of Emitted Particles

The predictions of the average numbers of nucleons that are emitted in the cascades generated in each of the model nuclei are shown in Tables III and IV. There are two interesting features of these results:

(a) If the effects of refraction are *excluded*, the average number of directly emitted particles is larger for the uniform-density model (SQUANO) than for the models with diffuse edges (TRAPNO and STEPNO).

(b) If refraction is included, the situation is entirely reversed and the model with the most diffuse edge (STEP) yields the greatest number of knock-on particles. The first observation demonstrates the significance of the relatively large central densities (see Fig. 1) that are found in the nuclear models with diffuse edges. The two observations taken together indicate the subtle interaction between the nuclear model used and the effects of refraction, referred to at the beginning of this section.

C. Average Excitation Energy

The complexity of the effects that accompany either a change of the nuclear model used or the inclusion of refraction is underlined by the changes in the average excitation energy as given in the last columns of Tables III and IV. The increase in the average excitation energy attendant upon the inclusion of refraction in each nuclear model is expected for the same reasons as were previously given for the concomitant decrease in transparency. The effects of density distribution on excitation energy are not so easily rationalized.

D. Spallation Reactions

One of the principal goals of Monte Carlo cascade calculations is the correct prediction of spallation-product yields from a wide variety of reactions. Unfortunately, such predictions depend not only on the cascade calculations but also on the manner in which the evaporative de-excitation of the cascade products is treated. In the present instance, the evaporation calculations were always performed by the Monte Carlo method described by Dostrovsky, Fraenkel, and Friedlander.[20] The computer program was kindly made available by N. T. Porile.

For a comparison of calculated and experimental data on a complete mass-yield curve we have chosen the interaction of As^{75} with 378-MeV protons studied experimentally by Cumming.[21] Qualitatively, the shape

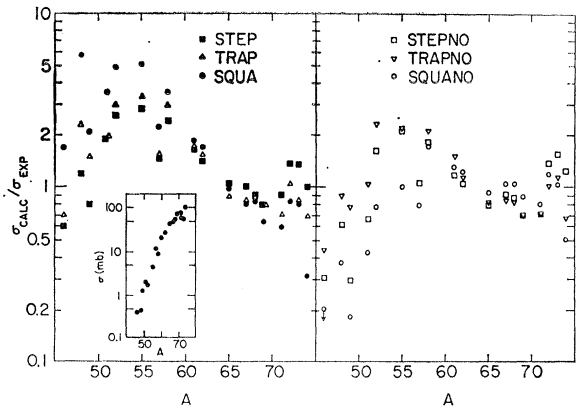

FIG. 2. Comparison of calculated and experimental mass-yield curves obtained in the interaction of As^{75} with 378-MeV protons. In the main body of the figure, the ratios of calculated to experimental cross sections are shown for the six models investigated. The inset shows the actual experimentally determined curve (Ref. 21).

of the mass-yield curve, with cross sections extending over three orders of magnitude (see inset in Fig. 2), is rather well reproduced by all VEGAS models. To show the degree of agreement or disagreement more clearly, ratios of calculated to experimental cross sections are plotted at each mass number in Fig. 2 for the six models. The "experimental" results are based on Cumming's data and include interpolated values for the cross sections of stable and long-lived products not observed by him. These interpolated values were obtained from the relative isobaric yields predicted by the evaporation calculations mentioned above. Experimental data are plotted only at those mass numbers where the measured contribution exceeded 50% of the total value.

Figure 2 shows that, for each of the density distributions, the predicted cross sections of simple reactions tend to be decreased, and those of complex spallation reactions are substantially increased when refraction effects are included; this is a direct consequence of the increased energy deposition. The over-all agreement between experiment and calculation is poorest for the SQUA and SQUANO models. The differences among the other four sets of results are probably not sufficiently large to allow a clearcut choice among them, except possibly for the simplest reactions, where the STEP and STEPNO models appear to be superior to the TRAP and TRAPNO models (see next section). It is not clear whether the peak in the $\sigma_{calc}/\sigma_{expt}$ curves near $A=55$ that is common to all the models except SQUANO represents a failure of the cascade calculations. It may well be a result of the manner in which the evaporation was treated. Preliminary calculations by Hillman[22] indicate that the inclusion of evaporation of particles heavier than He^4 in the calculations leads to a shift of the product spectra to lower masses for initial excitations above ~200 MeV; such an effect would qualitatively

[20] I. Dostrovsky, Z. Fraenkel, and G. Friedlander, Phys. Rev. 116, 683 (1960).

[21] J. B. Cumming, Ph.D. thesis, Columbia University, New York, 1954 (unpublished), and personal communication.

[22] M. Hillman (private communication).

give rise to a flattening of the $\sigma_{calc}/\sigma_{expt}$ curves below $A \approx 60$.

Comparisons between calculated and observed[23] excitation functions for some reactions of protons with Bi^{209} are shown in Figs. 3 and 4. The poor agreement between the experimental results and the calculation based on the STEP model again exemplifies the overestimation of the opacity of the nucleus at low incident energies that is evidently inherent in the STEP model. For example, at 95 MeV about 300 mb out of the calculated 400 mb for the production of Po^{202} (Fig. 3) comes from the evaporation of eight neutrons from compound nuclei that are formed in the cascade; the remaining 100 mb, a value that is not far from the observed value, arises from events in which at least one of the neutrons is directly ejected in the intranuclear cascade. A corollary of this difficulty is seen in the excitation function for the production of Pb^{203} that is shown in Fig. 4. Since the formation of Pb^{203} probably requires the direct ejection of at least one proton because the relatively large Coulomb barrier inhibits proton emission during the evaporation step, any model which underestimates the emission of cascade particles will underestimate the cross section for formation of Pb^{203}. The comparison shows that the STEP model consistently underestimates the Pb^{203} cross section, just as it consistently overestimates the Po^{202} cross section. Cross sections based upon STEPNO, which are also shown in Figs. 3 and 4, show better agreement with experiment than do those based upon STEP, but also leave something to be desired.

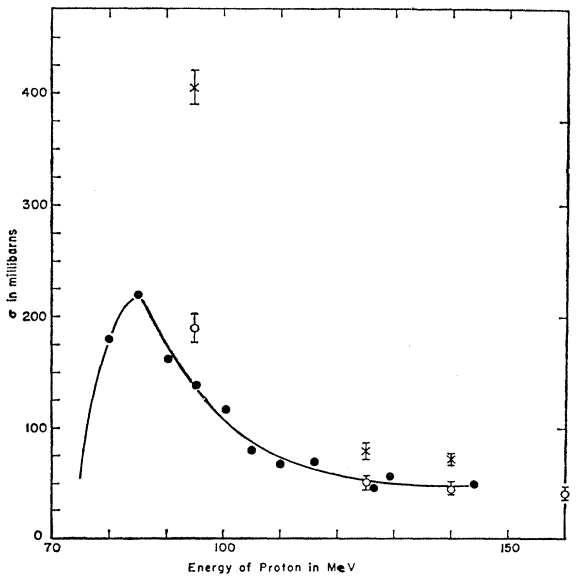

FIG. 3. Excitation function for the reaction $Bi^{209}(p,8n)Po^{202}$. The solid points are the experimental data of Ref. 23. The open circles and crosses are calculated with the STEPNO and STEP models, respectively.

[23] C. Brun and M. Lefort, J. Inorg. Nucl. Chem. 26, 1633 (1964), and personal communication.

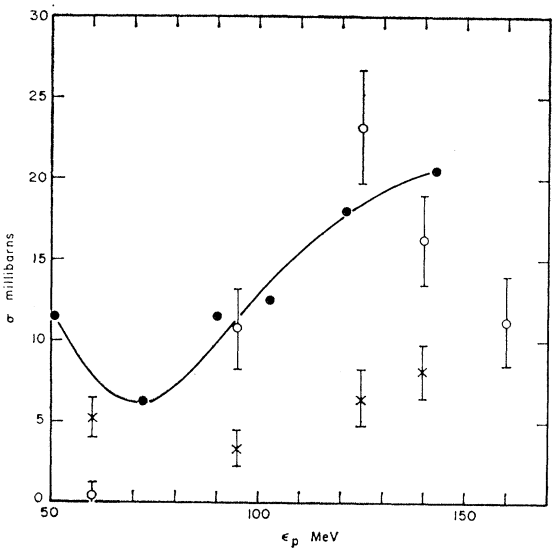

FIG. 4. Excitation function for the production of Pb^{203} by proton bombardment of Bi^{209}. The solid points are the experimental data of Ref. 23. The open circles and crosses are calculated with the STEPNO and STEP models, respectively.

E. "Simple" Reactions

As was mentioned by Metropolis *et al.*,[3] the large underestimation of the cross sections for simple nuclear reactions such as (p,pn), etc., was one of the outstanding failures of the SQUANO model. The suggestion made in Ref. 3 that this large discrepancy (a factor of $\sim$2–3) would be diminished by the introduction of a diffuse nuclear surface was borne out by Bertini's[4] investigation of a model similar to STEPNO. It was further found by Bertini that the introduction of an unrealistically large radius in the SQUANO model can also remove the discrepancy. This latter result is not surprising since, qualitatively, the probability of a (p,pn) reaction relative to more complex reactions should increase as the ratio of mean free path (λ) to radius (R) increases, and, since the mean free path varies approximately as R^3, this ratio (λ/R) varies about as R^2.

The effects of the diffuse surface and of refraction on simple nuclear reactions are illustrated in Table VI, where cross sections of various types of simple cascades with As^{75} and Bi^{209}, classified according to ejected particles and residual excitation energy, are given in mb for each of the six models investigated. The cross section, for example, of the (p,pn) reaction would approximately be given by the sum of the cross sections for the (P,PN) $(U<10)$ cascade and those fractions of the (P,P') $(10<U<20)$ and (P,N) $(10<U<20)$ cross sections which result in the evaporation of one and only one neutron or proton, respectively. A comparison of the appropriate quantities among the various models is in agreement with the result of Bertini on the effects of a diffuse surface. Further, it may be seen that the effects of the diffuse surface survive, although they are

TABLE VI. Calculated cross sections in mb for particular short cascades.

Target	Incident energy (MeV)	Type	Residual energy (MeV)	SQUANO	SQUA	TRAPNO	TRAP	STEPNO	STEP
As^{75}	378	*P,N*	$U<10$	1.5±0.7	1.5±0.7	4.2±1.2	2.3±0.9	7.2±1.9	4.6±0.9
			$10<U<20$	4.3±1.1	3.4±1.0	2.3±0.9	5.7±1.5	6.2±1.8	6.2±1.8
		P,P'	$U<10$	3.1±1.0	2.1±0.8	6.4±1.6	5.3±1.4	9.8±2.2	5.7±1.7
			$10<U<20$	8.3±1.6	8.6±1.6	9.1±1.8	12.8±2.2	13.4±2.6	10.8±2.4
		P,PN	$U<10$	16.5±2.2	9.2±1.7	26.8±3.2	25.3±3.1	53.0±5.2	40.1±4.5
			$10<U<20$	9.2±1.7	17.1±2.3	18.5±2.6	10.9±2.0	26.7±3.7	17.5±3.0
		P,2P	$U<10$	14.7±2.1	5.2±1.3	24.5±3.0	16.6±2.5	42.6±4.7	27.7±3.8
			$10<U<20$	12.9±2.0	6.1±1.4	8.7±1.8	10.9±2.0	19.0±3.1	9.3±2.2
		P,2N	$U<10$	0.6±0.4	none	none	0.75±1.5	0.5±0.5	1.0±0.7
			$10<U<20$	1.5±0.7	0.6±0.4	1.1±0.7	none	1.5±0.9	none
Bi^{209}	375	*P,N*	$U<10$	1.3±0.9	1.2±0.9	2.6±1.3	1.9±1.1	9.0±2.7	8.2±2.6
			$10<U<20$	3.7±1.5	6.2±2.0	7.1±2.1	5.8±1.9	13.1±3.3	9.9±2.8
		P,P'	$U<10$	3.1±1.4	5.0±1.8	5.2±1.8	5.2±1.8	8.2±2.6	18.1±3.8
			$10<U<20$	11.2±2.6	7.5±2.2	11.0±2.7	14.8±3.1	13.9±3.4	19.7±4.0
		P,PN	$U<10$	23.0±3.8	8.7±2.3	34.8±4.7	18.7±3.5	59.0±7.0	33.6±5.3
			$10<U<20$	21.2±3.7	10.0±2.5	19.4±3.5	8.4±2.3	20.5±4.1	15.6±3.6
		P,2P	$U<10$	18.1±3.4	3.1±1.4	23.8±3.9	12.3±2.8	41.0±5.8	22.2±4.3
			$10<U<20$	5.0±1.8	2.5±1.2	5.8±1.9	1.3±0.9	6.6±2.3	4.9±2.0
		P,2N	$U<10$	none	none	none	0.6±0.6	0.8±0.8	0.8±0.8
			$10<U<20$	none	0.6±0.6	3.2±1.4	none	1.6±1.2	3.3±1.0

diminished by, the introduction of refraction. The differences between the prediction of TRAPNO and STEPNO and between TRAP and STEP demonstrate the significance to these reactions of the details of the diffuse surface and in particular of the very outermost regions of the surface.

Comparison between measured and calculated[24] cross sections for two (p,pn) reactions are presented in Figs. 5 and 6. In Fig. 5 the excitation function[25] for the reaction $Au^{197}(p,pn)Au^{196}$ is compared with STEP and STEPNO calculations on the same reaction for another heavy nucleus, Bi^{209}. It is seen that STEPNO, which is similar to the Bertini calculation, is in good agreement with the experimental results, while the introduction of refractive effects (STEP) causes a large divergence from experimental results, particularly at the lower bombarding energies. The same conclusion can be drawn from the comparison of experimental data[26] on the excitation function of the reaction $Cu^{65}(p,pn)Cu^{64}$ with STEP and STEPNO calculations shown in Fig. 6: again the STEP model leads to serious underestimates of the (p,pn) cross section at energies below ~200 MeV, whereas STEPNO gives good agreement. Furthermore, a comparison with the detailed breakdown of $\sigma_{p,pn}$ into the contributions from different mechanisms by Grover and Caretto[8] shows that the discrepancy found in STEP arises largely from an underestimate of the direct knock-out reaction (P,PN cascade with $U<10$ MeV) whereas the STEPNO calculation appears to reproduce their conclusions very well.

Reference to Table VI shows that cross sections for (p,pn) reactions calculated with the trapezoidal density distribution are smaller than those calculated with the step distribution and thus will not agree as well with the experimental results. This observation again emphasizes the importance to these reactions of the outermost regions of the nucleus.

F. Energy and Angular Distribution of Emitted Particles

The emission of high-energy particles is a signature of the direct processes which occur in high-energy nuclear reactions and provides the most detailed test for any models of these reactions. The six models that were studied in this calculation do not, in general, predict marked differences for the energy and angular distribution of the protons emitted from the interactions, for example, of 375-MeV protons with As^{75} and Bi^{209}. The main qualitative difference is found in the increased probability for the emission of protons with energies greater than 90 MeV at angles greater than about 120° when refraction is included in the calculation with any of the density distributions. This enhanced emission of high-energy nucleons at backward angles is a straight-

[24] The contribution to the calculated cross section of nucleon evaporation from excited cascade products was estimated in the same way as described for spallation reactions in Sec. IV D.

[25] H. P. Yule and A. Turkevich, Phys. Rev. 118, 1591 (1960).

[26] A. A. Caretto, U. S. Atomic Energy Commission Report No. NYO-10693 (1964) (unpublished).

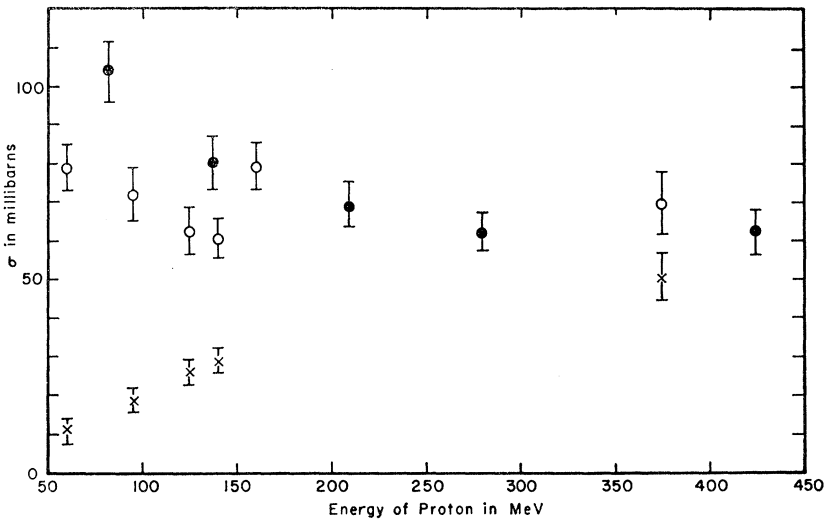

FIG. 5. Excitation function for the production of Au^{196} by proton bombardment of Au^{197}. The solid points are the experimental data of Ref. 25. The open circles and crosses are calculated with the STEPNO and STEP models, respectively, for production of Bi^{208} from Bi^{209}.

forward consequence of the possibility of reflection of cascade particles at the nuclear surface.

A comparison between the calculated and the observed[27] angular distribution of high-energy (>90 MeV) protons emitted in the inelastic interaction of 310-MeV protons with AgBr is shown in Fig. 7. There it can be seen that the STEP model faithfully reproduces the forward peaking of the protons as well as the rate of falloff at larger angles. The relatively small number of events that were observed in this experiment does not provide information about high-energy protons emitted at angles greater than 120° and thus does not provide criteria for distinguishing among the models. More detailed measurements of differential cross sections for emitted protons are clearly desirable.

The situation is significantly different when the kinetic energy of the incident particle is reduced to below about 200 MeV. In particular, the neglect of refraction introduces a broad high-energy peak in the energy spectra in the forward direction. This peak is greatly diminished upon the introduction of refraction. Two examples of this effect are given in Figs. 8 and 10. A comparison between the observed[28] and calculated energy spectra of protons emitted at 30° from the interactions of 160-MeV protons with Bi^{209} is shown in Fig. 8 in which are also plotted the data of Genin *et al.*[29] for Au^{197}+154-MeV protons. It is evident that, at 30°, the calculation based upon the STEPNO model is in substantially better agreement with these experimental results than is that based on the STEP model. However, in a recent paper, Brun *et al.*[30] reported a spectrum of protons emitted at 25° in the interactions of 156-MeV protons with gold which was essentially flat at 2 mb MeV^{-1} sr^{-1} from 30 to 150 MeV. Similar experiments by Peele[31] gave results that differ from both of the other

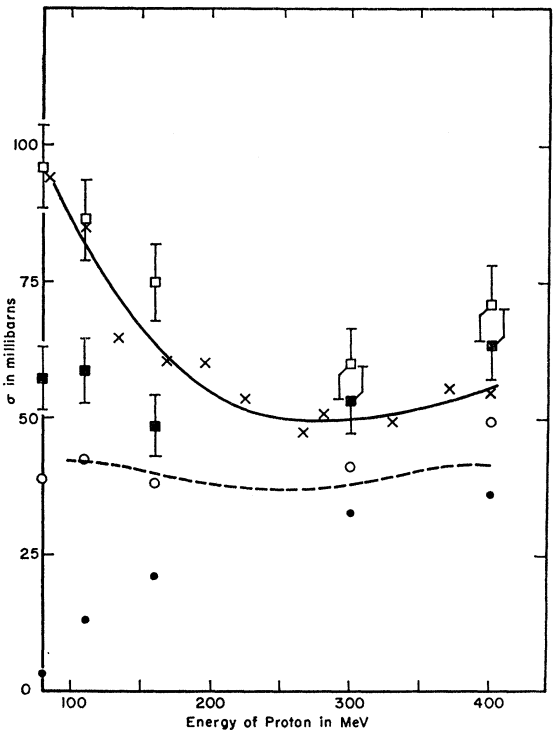

FIG. 6. Excitation function for the production of Cu^{64} by proton bombardment of Cu^{65}. ×, experimental data from Ref. 26; □, (p,pn) cross section calculated with STEPNO; ■, (p,pn) cross section calculated with STEP; ○, knockout contribution calculated with STEPNO; ●, knockout contribution calculated with STEP. The solid curve is drawn through the experimental data. The dashed curve represents the knockout contribution estimated by Grover and Caretto (Ref. 8) from (p,p') data.

[27] J. Friedman (unpublished), as reported in Ref. 3.

[28] P. G. Roos, Ph. D. thesis, University of Maryland, College Park, 1964 (unpublished), and personal communication from S. Wall.

[29] J. Genin, P. Radvanyi, I. Brissaud, and C. Detraz, J. Phys. Radium **22**, 615 (1961).

[30] The experimental results reported by Bowen *et al.*, in Ref. 33 are given only in arbitrary units. The normalization to mb sr^{-1} MeV^{-1} is based upon information provided by the experimenters and transmitted to the authors through H. Bertini.

[31] C. Brun, H. Dubost, B. Gatty, M. Lefort, and X. Tarrago, Nucl. Phys. **A95**, 337 (1967).

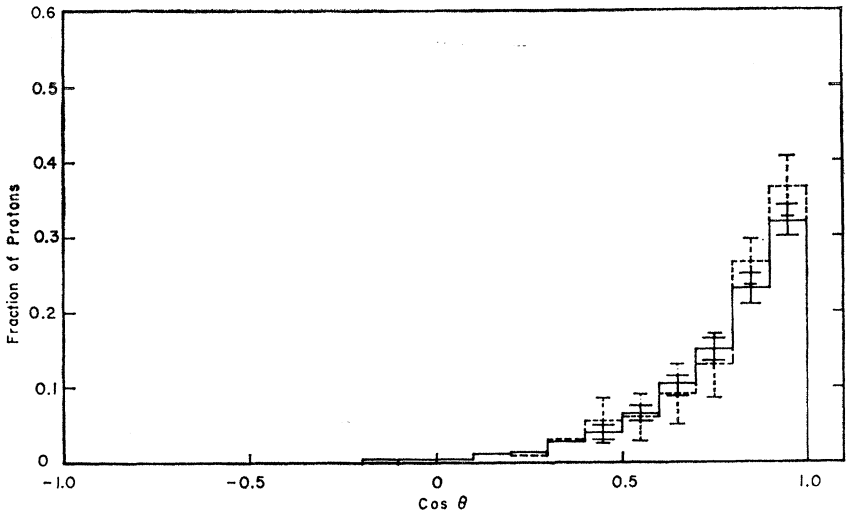

FIG. 7. Angular distribution of fast ($\geq$90 MeV) protons emitted in the interaction of 310-MeV protons with AgBr. The dashed histogram represents the experimental data obtained by Friedman for 682 stars in photographic emulsions (Ref. 27); the solid histogram is the result of a STEP-model calculation with 916 inelastic events in Ag and 911 in Br.

sets of data mentioned, but are somewhat closer to those of Brun *et al.* In view of these experimental disagreements it is difficult to use these data as a critical test of the calculations.

The divergence among experimenters becomes much less at larger angles. Also, the agreement between calculated and experimental results improves at larger angles, as can be seen in Fig. 9 for the 80° spectrum of protons from Bi^{209}+160-MeV protons. Here the STEP model may give slightly better agreement with experiment than does STEPNO, particularly for the high-energy tail. As was pointed out before, the presence or absence of a high-energy tail in the proton spectra at large angles is a persistent difference between calculations based upon the STEP and the STEPNO models.

The energy spectrum[32] of the neutrons emitted in the forward direction in the interaction of Pb^{207} with 143-MeV protons[33] is compared with calculations based upon the STEP and the STEPNO models in Fig. 10. This comparison shows an impressive disagreement with the calculations based upon both the STEP and the STEPNO models. Interestingly, the *shape* of the spectrum based upon the STEP model agrees with experiment better than that based upon STEPNO.

The comparison between experimental[28] and calculated results shown in Fig. 11 for the energy spectrum of protons emitted at 30° in the interaction of 160-MeV

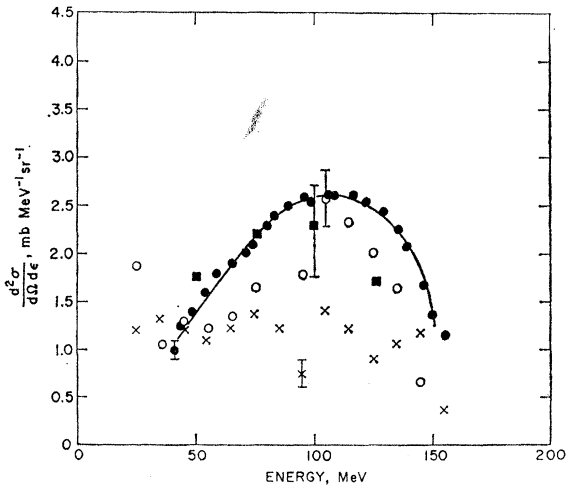

FIG. 8. Differential cross section for protons emitted at 30° in the laboratory system in the interaction of 160-MeV protons with Bi^{209}. The solid circles are the experimental data of Roos and Wall (Ref. 28), the open circles and crosses were obtained from the STEPNO and STEP calculations, respectively. The data of Genin *et al.* (Ref. 29) for 154-MeV protons on Au^{197} are also shown (squares). For some representative points, errors (standard deviations in case of the calculated data) are shown.

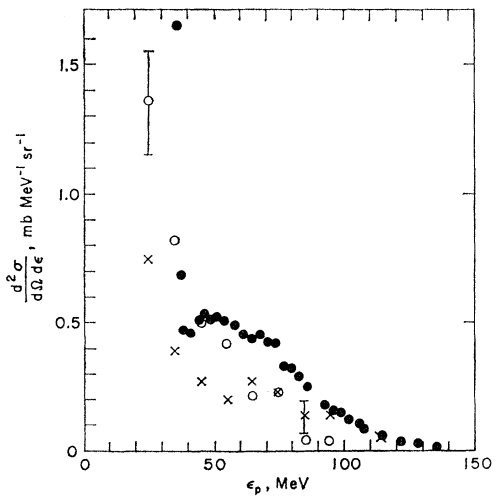

FIG. 9. Differential cross sections for protons emitted at 80° in the laboratory system in the interaction of 160-MeV protons with Bi^{209}. Symbols have same meaning as in Fig. 8.

[32] R. Peele (private communication).

[33] P. H. Bowen, G. C. Cox, G. B. Huxtable, J. P. Scanlon, J. J. Thresher, and A. Langsford, Nucl. Phys. **30**, 475 (1962).

protons with Ni^{58} shows better agreement than that for Bi. The shape of the experimental spectrum is somewhat better reproduced by the STEPNO than by the STEP model.

In summary, it may be said that the discrepancies between observed and calculated energy and angular distributions for incident energy of $\lesssim 150$ MeV suggest an inadequacy in the treatment of directly emitted particles of the second and later generations: The calculation gives too few of them. This remark is particularly true for calculations based upon the STEP model and for high-Z targets.

G. Linear Momentum Transfer

The dependence of the average linear momentum transfer on the excitation energy of the cascade product is a quantity that is of interest in the interpretation of recoil experiments.[34] This relation might be expected to depend in a complex way on target mass number, bombarding energy, and number of ejected cascade particles. In actual fact, the VEGAS calculations indicate that some fairly broad generalizations can be made.

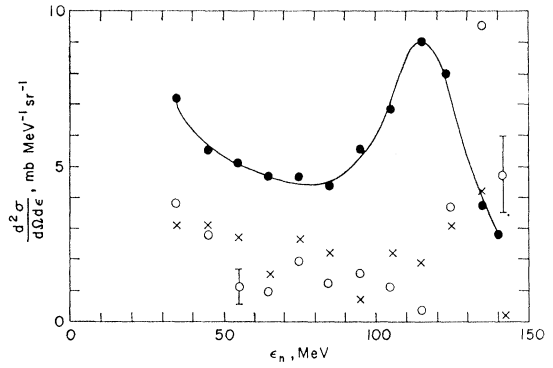

FIG. 10. Differential cross sections for neutrons emitted in the forward direction in the interaction of 143-MeV protons with Pb^{207}. The solid circles represent the data of Bowen *et al.* (Ref. 33) taken at 0°; the open circles and crosses are the results of STEPNO and STEP calculations, respectively, for the angular interval 0°–8°.

For one thing, the predicted average forward momentum transfer $\bar{p}_{11}$ as a function of excitation energy E^* is practically independent of the model used. This is illustrated in Fig. 12, where the ratio of $\bar{p}_{11}$ to the incident momentum p_{inc} is plotted against E^* for the STEP, STEPNO, and SQUANO model calculations of As^{75}+378-MeV protons. The data can be fairly well represented by a straight line going through $\bar{p}_{11}/p_{\text{inc}}=0$ at $E^*=0$ and through $\bar{p}_{11}/p_{\text{inc}}=1$ at $E^*=E_{\max}^*$ (where $E_{\max}^*$ is the excitation energy of a compound nucleus). A small but significant difference between the models with and

[34] See, e.g., V. P. Crespo, J. M. Alexander, and E. K. Hyde, Phys. Rev. 131, 1765 (1963); J. B. Cumming, S. Katcoff, N. T. Porile, S. Tanaka, and A. Wyttenbach, *ibid.* 134, B1262 (1964); N. Sugarman, H. Münzel, J. A. Panontin, K. Wylgoz, M. V. Ramaniah, G. Lange, and E. Lopez-Menchero, *ibid.* 143, 952 (1966).

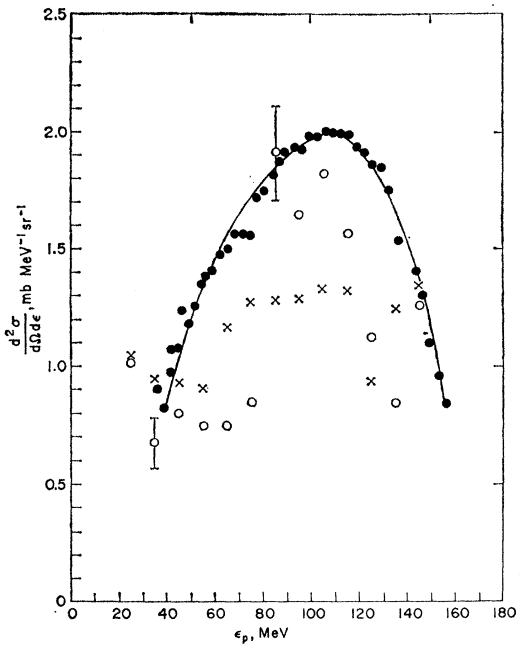

FIG. 11. Differential cross section for protons emitted at 30° in the interaction of 160-MeV protons with Ni^{58}. The solid circles represent the data of Roos and Wall (Ref. 28); the open circles and crosses are the results of STEPNO and STEP calculations, respectively.

without refraction appears at low excitations, where refraction effects give rise to increased momentum transfers.

The last-mentioned effect is seen clearly in Fig. 13,[35] which shows the correlation between p_{11} and E^* for interactions between 380-MeV protons and U^{238} calculated with the STEP model. The data are represented in two different ways: in terms of $\bar{p}_{11}/p_{\text{inc}}$ at given values of $E^*/E_{\max}^*$, and in term of $\bar{E}^*/E_{\max}^*$ at given values of p_{11}/p_{inc}. The two curves are seen to be very different. The $\bar{E}^*/E_{\max}^*$ data extend to negative values of p_{11} (backward recoils) and to p_{11}/p_{inc} values >1. As p_{11}/p_{inc} increases above unity, $\bar{E}^*/E_{\max}^*$ decreases because these very large forward momentum transfers must be

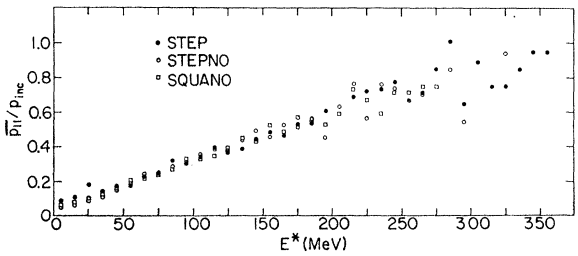

FIG. 12. Average forward momentum of cascade products as a function of their excitation energy for the interaction of 378-MeV protons with As^{75}. The momenta are given in units of the incident momentum. Results are given for three models.

[35] N. T. Porile, Phys. Rev. 120, 572 (1960).

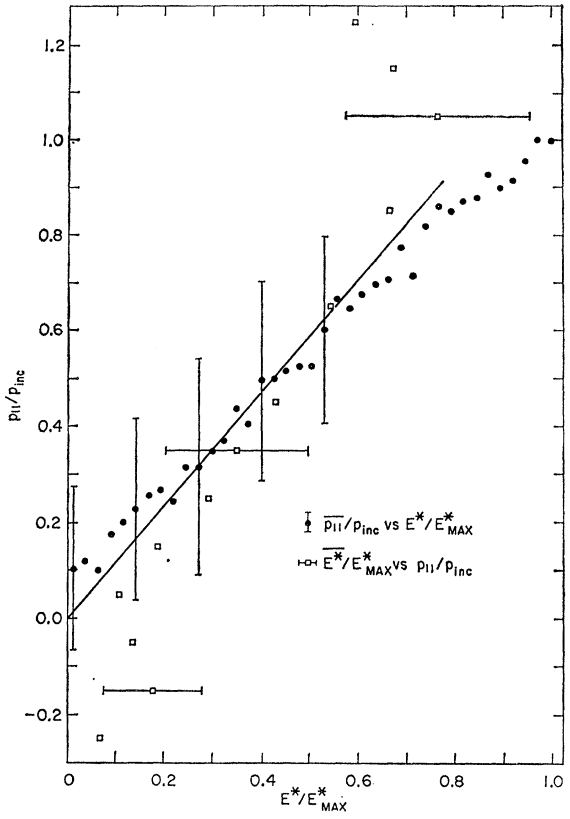

FIG. 13. Correlation between forward momentum and excitation energy of cascade products in the STEP model simulation of the interaction of 380-MeV protons with U^{238}. Both the average values of p_{11} in given excitation energy intervals (closed circles) and the average values of E^* in given intervals of p_{11} (open squares) are shown. The momenta are given in units of the incident momentum p_{inc}, the energies in units of the compound nucleus excitation $E_{max}{}^*$. Root-mean-square deviations of the distributions are shown for some points. The line drawn is taken from Porile (Ref. 35) and applies to 460-MeV-proton interactions with U^{238}.

accompanied by large amounts of backward emission of cascade particles.

Another significant point is illustrated in Fig. 13: The distributions of momentum transfer for a given excitation-energy interval and of excitation energy for a given momentum-transfer interval are quite broad, the rms deviation often being of the same magnitude as the average value.

The results for $\bar{p}_{11}/p_{inc}$ versus $E^*/E_{max}{}^*$ are remarkably independent of both target mass number and proton energy. The principal effect of decreasing proton energy (in the models with refraction) is found in somewhat larger $\bar{p}_{11}/p_{inc}$ values at low excitations. This is shown in Fig. 14, where the $\bar{p}_{11}/p_{inc}$ curves for 155- and 380-MeV protons on U^{238} are compared.

Whereas $\bar{p}_{11}$ tends to increase approximately linearly with E^*, almost independently of model, the average momentum transfer perpendicular to the beam direction $\bar{p}_\perp$ varies much less with E^* and shows much greater refraction dependence. The $\bar{p}_\perp$ values at low excitations ($E^*<50$ MeV) are substantially higher when refraction is included than when it is not. At higher excitations the model differences tend to vanish, and the $\bar{p}_\perp/p_{inc}$ versus $E^*/E_{max}{}^*$ curves tend to be rather flat. These trends are found in the gross cascade products but they also show up in individual cascade products. This is shown in Fig. 15 for the $A=74$ cascade products formed from 378-MeV proton interactions with As^{75}. Again the distributions around the $\bar{p}_\perp$ values are very broad, as shown in Fig. 15.

H. Angular-Momentum Transfer

The dependence on excitation energy of the angular-momentum distribution of the cascade products is another quantity that is of significance to an understanding of the details of high-energy nuclear reactions. As for linear momentum, it is again found that the computed distributions are rather insensitive to the density distribution that is used, whereas the inclusion of refraction tends to increase the angular-momentum transfer (see Fig. 16).

In Fig. 16 are shown the average angular momenta of cascade products as a function of their excitation energies obtained in the STEP and STEPNO calculations for As^{75}+378-MeV protons and in STEPNO calculations for As^{75}+160-MeV protons. The large rms deviations from the mean values reflect both the distribution in impact parameters and the effects of the emitted cascade particles. It is worthy of mention that the angular-momentum distributions for a particular cascade product (e.g., As^{74} from As^{75}+378-MeV protons) are almost indistinguishable from those for the gross products.

I. Summary

Evidently, the effects introduced by refraction are, in general, more pervasive than those introduced by a change in the nuclear-density distribution. An important exception to this generalization is found in the

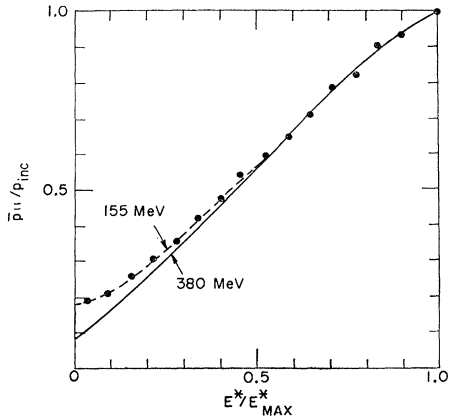

FIG. 14. Comparison of $\bar{p}_{11}/p_{inc}$ versus $E^*/E_{max}{}^*$ correlations for the interactions of 155- and 380-MeV protons with U^{238}.

effects of density distribution on simple reactions as illustrated in Table VI. The principal effects of refraction are an increase in excitation energy deposition and in linear- and angular-momentum transfer, and a corresponding decrease in the emission of secondary cascade particles. When compared with experiment, it is seen that the introduction of refractive effects increases the divergence between calculated and experimental values found, particularly for incident energies below ~200 MeV and for high-Z targets. At higher incident energies and for low- and medium-Z targets, a clearcut decision between calculations with and without refraction is at present not possible.

On the whole, the STEPNO model seems to give the best agreement with experimental data, although TRAPNO would probably be just about as good except, as may be seen in Table VI, for the "simple" reactions. The SQUA and SQUANO models are, as expected, clearly inferior.

V. DISCUSSION

The fact that calculated and experimental results for high-Z targets and low incident energies show better agreement when refraction and reflection of cascade particles are arbitrarily ignored than when they are included in the calculations is puzzling, and it would be desirable to understand the source of this unsatisfactory situation. Within the general framework of the model, there are two general classes of explanation. (a) The potential used is incorrect. (b) The classical treatment of refraction and reflection is a poorer approximation than is complete neglect of the effect. The latter possibility has been partially investigated by a comparison between a quantum-mechanical and a classical estimation of transmission coefficients[36] T_l as a function of orbital angular momentum of the incident particle; this investigation was carried out by Harp and Miller.[37] The quantum-mechanical calculation was made with the ABACUS II program of Auerbach[38] using optical-model parameters which were consistent with the corresponding quantities in the VEGAS calculation:

$$V_{op}=V_v-\hbar^2/8\mu\lambda^2 \tag{11}$$

$$W_{op}=-\frac{\hbar}{\lambda}\left(\frac{\mathcal{E}+V_v}{2\mu}\right)^{1/2}, \tag{12}$$

where $\mathcal{E}$ is the kinetic energy of the incident particle at infinity; μ is the reduced mass of the system; $\mathcal{E}+V_v$ and λ are, respectively, the kinetic energy and the mean free path of a cascade particle at a given point in the nucleus in the classical calculation; and V_{op} and W_{op} are the corresponding depths of the real and imaginary parts of the optical potential at the same point in the nucleus. The particular values for the real and imaginary parts of the optical potential given in Eqs. (11) and (12) arises from the condition that the mean free path and momentum of the particle at each point

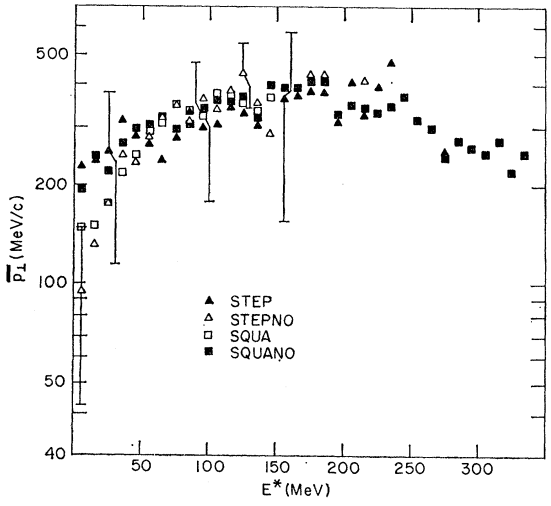

FIG. 15. Average momentum of As^{74} cascade products perpendicular to the beam direction, plotted as a function of excitation energy deposited in the interaction of 378-MeV protons with As^{75}. Results for four models are compared.

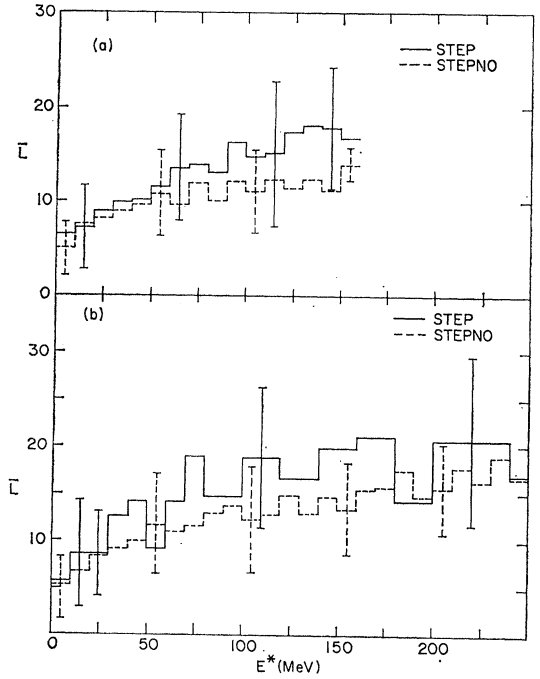

FIG. 16. Calculated average angular momenta of residual nuclei produced in proton interactions with As^{75}. The top graph is for incident protons of 160 MeV, the bottom graph for 378-MeV protons. The maximum angular momenta carried in by the incident protons at these two energies are 21 and 33 units of $\hbar$, respectively.

[36] The transparency in the VEGAS calculation is $1-T_l$.

[37] G. Harp and J. M. Miller, Columbia University Report No. CU-1019-49, 1966 (unpublished).

[38] E. Auerbach, Brookhaven National Laboratory Report No. BNL 6562, 1962 (unpublished).

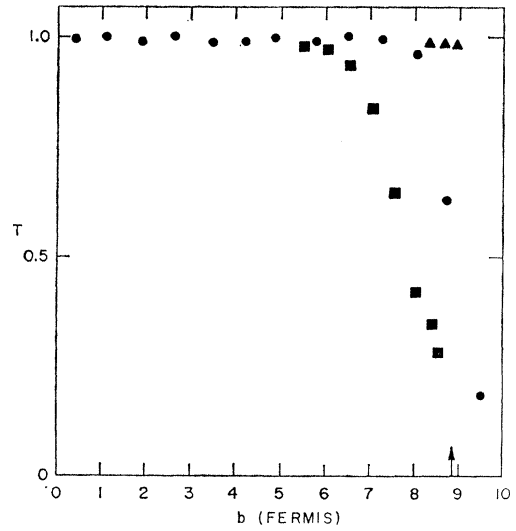

FIG. 17. Transmission coefficients (or 1 minus probability of a transparency) for 50-MeV-proton interactions with Bi^{209}, plotted against impact parameter b of proton at the nuclear surface (Ref. 37). Circles are from a quantal calculation, squares are from a classical calculation without refraction, triangles are from a classical calculation with refraction.

in the nucleus be the same in the classical and quantal calculations: The complex propagation vector k of the quantal solution should have the magnitude

$$k=[2\mu(\mathcal{E}+V_0)/\hbar^2]^{1/2}+i/2\lambda. \quad (13)$$

The classical values of the transmission coefficients were computed analytically from the classical trajectories and the mean free path in each region. From the results of this comparison shown in Figs. 17 and 18 for 50- and 160-MeV protons, respectively, incident on Bi^{209}, it is evident that the results of the quantal calculation fall between those of the classical calculations of transmission coefficients with and without refraction. At the lower energy the classical calculation with refraction reproduces the quantal calculation somewhat better than does that which neglects refraction. Thus the classical approximation to refraction and reflection is apparently not the primary source of the divergence between results from the STEP model and experimental observation. This leaves the first alternative: the use of an unrealistic potential for the cascade particles.

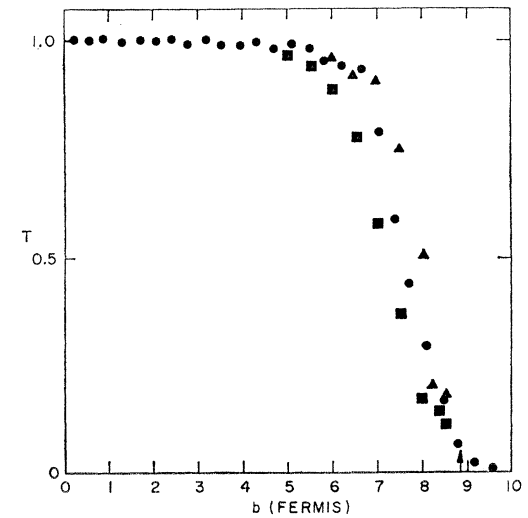

FIG. 18. Same as Fig. 17, but for 160-MeV protons incident on Bi^{209}.

As discussed in Sec. II, the nuclear potential energy used in the VEGAS calculation is completely determined by the assumed nuclear density distribution and is taken to be independent of the energy of the cascade particle. There is, however, abundant evidence from optical-model analyses[39] of elastic-scattering and cross-section data that the depth of the potential well diminishes with increasing particle energy, an effect that would bring the STEP and STEPNO calculations closer together. Accordingly, the consequences of using a velocity-dependent potential for the refraction and reflection of the cascade particles are under investigation.

ACKNOWLEDGMENTS

This work was done while one of the authors (Z.F.) enjoyed the hospitality of the Brookhaven National Laboratory Chemistry Department. Helpful discussions with many colleagues, in particular with H. Bertini, I. Dostrovsky, N. Metropolis, A. Turkevich, N. Warszauer, and C. Zerby, are gratefully acknowledged.

APPENDIX: SELECTION OF COLLISION PARTNER AND SITES

In this Appendix the method of selection of collision partner and sites will be discussed in some detail for a uniform-density nucleus and the straightforward extension to the varying-density models will then be outlined.

The Lorentz-invariant probability of interaction between one beam of identical particles with momentum $\mathbf{p}_1$ and density ρ_1 and a second beam of particles with momentum $\mathbf{p}_2$ and density ρ_2 per unit 4-space is given by[40]

$$P=\sigma_{12}\rho_1\rho_2 v_{12},$$

where v_{12} is the relative velocity of the two beams with respect to each other and σ_{12} is the cross section of interaction between a particle of beam 1 with momentum $\mathbf{p}_1$ and a particle of beam 2 with momentum $\mathbf{p}_2$.

Suppose now that the second beam does not consist of particles of equal momentum but of particles of a continuous momentum distribution. In this case the probability of interaction per unit 4-space for a given

[39] See, e.g., P. E. Hodgson, *The Optical Model of Elastic Scattering* (Oxford University Press, New York, 1963).

[40] F. J. Belinfante and C. Møller, Kgl. Danske Videnskab. Selskab, Mat.-Fys. Medd. 28, Paper 6 (1954).

momentum $\mathbf{p}_1$ is

$$P(p_1)=\rho_1\int\sigma_{12}(\mathbf{p}_2)v_{12}(\mathbf{p}_2)\frac{\partial\rho_2}{\partial\mathbf{p}_2}d\mathbf{p}_2, \tag{A1}$$

where the integration is performed over the continuous particle distribution of beam 2. Assume next that beam 1 is the beam of the bombarding particles whereas beam 2 consists of the nucleons of the bombarded nucleus. Then the momentum distribution of beam 2 would be the momentum distribution of the nucleons in a nucleus. Consider now a single bombarding particle entering the nucleus. The probability per unit path length of the particle to interact with the nucleons of the nucleus is

$$Q=\frac{P(p_1)}{\rho_1 v_1}=\frac{1}{v_1}\int\sigma_{12}v_{12}\frac{\partial\rho_2}{\partial\mathbf{p}_2}d\mathbf{p}_2=\lambda_1^{-1}, \tag{A2}$$

where v_1 is the laboratory velocity of the bombarding particle and λ_1 is, then, its mean free path. The probability of the bombarding particle to interact at a distance between a and $a+da$ is

$$dN(a)=e^{-Qa}Qda. \tag{A3}$$

Since the dependence of σ_{12} on v_{12} (i.e., energy dependence of the cross section) cannot normally be expressed in a closed functional form, the evaluation of Q must in general be done by numerical integration

$$Q\simeq\frac{1}{v_1}\sum\sigma_{12}v_{12}\frac{\partial\rho_2}{\partial\mathbf{p}_2}\Delta\mathbf{p}_2. \tag{A4}$$

If the nucleon distribution is assumed to be that of a degenerate Fermi gas, a convenient method of calculation is to divide the Fermi sphere of momentum into n parts of equal volume and calculate the mean cross section σ_{12} and the mean velocity v_{12} for each subvolume. If Q is calculated in the rest system of the nucleus, the momentum distribution in question is the "undistorted" Fermi gas distribution for each subvolume $(\delta\rho_2/\delta\mathbf{p}_2)\Delta\mathbf{p}_2=\rho/n$;

$$Q\simeq\frac{1}{v_1}\sum_{i=1}^{n}\sigma_{12_i}v_{12_i}\Delta\rho_i=\frac{\rho}{n}\sum_{i=1}^{n}\sigma_i', \tag{A5}$$

where

$$\sigma_i'=(v_{12_i}/v_1)\sigma_{12_i}. \tag{A6}$$

The calculation may now proceed in several ways. The method previously used is to determine the site of the next collision by a partial integration of Eq. (A3) (over variable a) and choose the collision partner by a partial integration of the normalized equation (A4). We have already pointed out that this method for determining the collision site cannot be used if the cascade is followed on a timelike basis. A method which would be satisfactory for the purpose is (a) determine whether a collision has taken place in a given interval a by comparing a random number with the partial integration of Eq. (A3) between zero and a. If this comparison determines that a collision has taken place, (b) the site of the collision and (c) the collision partner are chosen in the usual way. The partial integration of Eq. (A3) may be written in the following form [using the approximation of Eq. (A5)]

$$N(a)=1-\exp(-Qa)=1-\prod_{i=1}^{n}\exp\left(-\frac{a}{n}\rho\sigma_i'\right). \tag{A7}$$

Each term of the product on the right side of Eq. (A7) is formally equivalent to the probability of no collision between the cascade particle and a beam of particles of momentum $\mathbf{p}_i$ and density ρ occurring in an interval a/n. In other words, the probability of a collision of the cascade particle in the interval a may be calculated by dividing the interval a into n equal parts and calculating for each interval $\delta a=a/n$ the probability of collision between the cascade particle and a hypothetical nucleon gas having a density ρ (the total nucleon density) and nucleon momentum $\mathbf{p}_i$. For each interval a/n, a different momentum $\mathbf{p}_i$ is chosen out of the undistorted momentum distribution so that each momentum $\mathbf{p}_i$ represents one subvolume ρ/n of this distribution. The sequence in which the various momenta p_i are chosen is of course completely arbitrary. We may combine steps (a)–(c) of the calculation in the following way: The interval a is divided into n equal parts. A momentum $\mathbf{p}_i$ is chosen at random out of the Fermi distribution and each choice of a momentum is associated with a small step a/n forward of the cascade particle; a test is then made to see if the collision occurs in that step by the comparison of a random number to the quantity

$$N(\delta a)=1-\exp(-\rho\sigma_i'\delta a), \tag{A8}$$

where σ_i' is chosen appropriately by interpolation from Tables I or II (see Sec. III A). Interpreting our method in terms of the three steps outlined above we may say that step (a) [the numerical integration of Q, Eq. (A5), followed by the calculation of the partial integrations of $dN(a)$, Eq. (A3)] is replaced by an indirect Monte Carlo integration of Eq. (A5). Step (b) (choice of collision site) is performed by dividing the interval a into n equal parts and checking whether a collision has taken place in each of them. Finally step (c) (the choice of a collision partner) is carried out by a rejection technique whereby a momentum $\mathbf{p}_i$ is chosen at random and the probability of interaction with a collision partner of this momentum is compared with a second random number.

Our method of choosing the collision site and partner may seem to be unnecessarily complicated. It has, however, a number of advantages: The advance of the cascade particle in small steps δa is particularly convenient if the cascade is to be followed on a timelike basis as will be seen below. The fact that the collision

site is chosen by checking for its occurrence in a series of small intervals δa (for each of which $\rho\sigma_i'\delta a \ll 1$) rather than checking once in a large interval a, allows us to use the linear approximation

$$N(\delta a) \simeq \rho\sigma_i'\delta a \tag{A9}$$

for determining both the collision site and the collision partners, and hence an appreciable saving of computer time is achieved.[41] Finally the choice of the collision partner by a rejection technique allows us to choose its momentum out of the undistorted nucleon distribution (i.e., the nucleon distribution as measured in the rest system of the nucleus) rather than choosing the momentum out of the distribution as given by the integrand in Eq. (A1) (the so-called distorted momentum distribution).

So far we have not discussed the size of the interval a and the number n of momentum samples to be chosen in this interval. The interval a is the path length over which a good estimate (on the average) of Q is required. A good choice for a would therefore be the mean free path λ between two collisions. Since in our calculation the value of $\lambda = Q^{-1}$ is never calculated explicitly we may choose $a = \tilde{\lambda}$;

$$\delta a = \tilde{\lambda}/n, \tag{A10}$$

where $\tilde{\lambda}$ is an *estimate* of the mean free path of the particle. The value to be chosen for n will in general depend on the accuracy required and on the type and energy of the interacting particles. The higher the accuracy required and the larger the variation of cross section with energy, the larger n must be. The actual choice of n is governed by three different considerations: (a) n must be large enough for the sampling method of the nuclear momentum distribution to provide a good estimate of the integral in Eq. (A2). This, however, does *not* mean that n must be large enough so that a good estimate of the integral is obtained between any two interactions of a given cascade particle. It does mean that if M complete nuclear cascades are to be followed, a good estimate of the integral should be obtained over these M cascades. Hence to some extent a lower value for n may be compensated by following a larger number of cascades. (b) Quite apart from the evaluation of the integral, the intervals δa must be small enough to retain the advantages of following the cascade particles on a timelike basis. These advantages would be lost if large changes in the positions and directions of the particles occurred in a single step. (c) Finally, if the linear approximation in Eq. (A9) is to be used, $\rho\sigma_i'\delta a$ must always be much smaller than unity.

[41] It should be emphasized that if $N(a)$ is calculated by a product of exponentials as in Eq. (A7) the linear approximation for each step cannot be used since the errors of all steps add. This is not the case in our procedure. Here a random number ζ is compared with $\rho\sigma_i'$ and since δa is so chosen that $\rho\sigma_i'\delta a \ll 1$ we find that for most intervals $\zeta > \rho\sigma_i'\delta a$ and no collision takes place. However, since $1-\exp(-\rho\sigma_i' da) < \rho_i'\delta a$, the same result would have been obtained if the random number would have been compared with the accurate (i.e., exponential) expression for $N(\delta a)$.

While it is relatively simple to arrive at a value of n which would satisfy criteria (b) and (c), it is more complicated to obtain *a priori* a value of n which would satisfy criterion (a). The way n was actually chosen was to calculate several hundred cascades each with $n=10$, 20, and 30 for a representative nucleus and bombarding energy. It was found that while increasing n from $n=10$ to $n=20$ did change the results of the calculation in a nontrivial fashion, the results of $n=20$ and $n=30$ did not differ outside the statistical fluctuations. It was hence decided to use $n=20$.

Once the approximate value of λ and n are determined, the Monte Carlo calculation effectively proceeds as follows: At the beginning of the interval the interaction partner is chosen to be a proton or a neutron according to the relative density of protons and neutrons in the nucleus $[\rho_p = \rho Z/A\,;\ \rho_n = \rho(A-Z)/A]$. Next the momentum $\mathbf{p}_2$ of the partner is chosen at random out of the appropriate (neutron or proton) Fermi sphere. With the density of the partner particle taken to be equal to the *total* nucleon density in the nucleus, the probability of at least one interaction in the interval $\tilde{\lambda}/n$ is calculated by Eq. (A9). A random number ζ is chosen and if $\zeta \leqslant N(\delta a)$, an interaction is assumed to have occurred. If $\zeta > N(\delta a)$, no interaction is assumed to have occurred, and the cascade particle is advanced by a distance $\tilde{\lambda}/n$. A new partner is chosen by the same method as in the previous interval and the process of determining whether an interaction took place is repeated. Suppose now that for a given interval i, $\zeta_i \leqslant N_i(\delta a)$ and an interaction has occurred. The distance X_i from the beginning of the interval to the point of interaction is then determined by

$$\zeta_i = 1 - \exp[-X_i\rho\sigma_i'], \tag{A11}$$

for which we may take the linear approximation

$$X_i \simeq \zeta_i(\rho\sigma_i')^{-1}. \tag{A12}$$

While the distance $\tilde{\lambda}/n$ would be a good choice for the interval for any given cascade particle, the actual value of δa will in general be smaller because the method of following the cascade particles on a timelike basis requires that the distances δa_i of *all* the cascade particles which are followed at a given time should correspond to the same time interval τ. Hence it is actually not the distances δa or $\tilde{\lambda}/n$ which are chosen but a time interval τ, and this time interval is common to all cascade particles in question. The actual distance b_i for particle i which is determined in this way is $b_i = \beta_i\tau$, where β_i is the velocity of particle i (in units of c).

The actual choice of the time interval τ proceeds as follows: At the beginning of the cascade the total cross sections σ_p and σ_n of the incoming particle with a stationary proton and a stationary neutron (in the lab system), respectively, are determined. An approximate mean free path $\tilde{\lambda}$ of the incoming particle is then

calculated

$$\tilde{\lambda}=(A/\rho_{\max})[Z\sigma_p+(A-Z)\sigma_n]^{-1}, \qquad \text{(A13)}$$

where $\rho_{\max}$ is the *total* nucleon density. Equation (A13) gives a sufficiently good estimate of the mean free path for the selection of a time interval, if there are no resonances in σ_p or σ_n. The time interval τ is then obtained from

$$\tau=\tilde{\lambda}/n\beta,$$

where β is the velocity of the incoming particle. A candidate for an interaction partner is then selected at random out of the momentum distribution. The next step is to determine whether an interaction has taken place in the path length $b=\beta\tau$ in the manner explained above. If no interaction has taken place, the particle is advanced by the path length b, a new value τ is calculated for the next time interval, and a new candidate for the interaction partner chosen and the process is repeated until the particle makes an interaction or escapes from the nucleus. If the Monte Carlo procedure determines that an interaction has taken place in a given time interval, the position of the interaction is determined by Eq. (A12) and the particle is advanced to this point. The angular distribution is then calculated by interpolating the values of Tables I or II to the correct energy, and a scattering angle is chosen by a rejection technique. Next the energy of the outgoing particles is determined. If either of the two energies is below the Fermi energy, the interaction is forbidden and the momentum of the incoming particle remains unchanged. A new candidate for interaction partner is, however, chosen and it is determined whether an interaction took place in the remaining time interval with the new partner. On the other hand, if the energies of both particles are above the Fermi energy, the interaction is allowed, and the momenta of the two outgoing particles are computed according to the chosen scattering angle. A candidate for interaction partner is then chosen for each particle and the possibility of interaction of either particle in the remaining time interval is determined in the usual fashion. The extension of this procedure to the simultaneous consideration of many cascade particles does not present any essential difficulties. At the end of each time interval a new candidate for an interaction partner is chosen and a new time interval $\tau_i=\tilde{\lambda}_i(n\beta_i)^{-1}$ is calculated for *each* particle and the smallest τ_i is then the one that is chosen for the next time interval

$$\tau=\min[\tau_i].$$

The procedure is somewhat different if a nuclear model with a nonuniform density distribution is under consideration: The density used in Eqs. (A9) and (A11) must be appropriate to the position of the cascade particle and the cascade particles must be refracted when they go through regions of changing density. Further, when a particle enters a region of different density in a given time interval τ, a check is first made of whether an interaction has taken place in the part of the path which lies in the old region. If no interaction took place, the particle is advanced to the end of the old region, the momentum of the particle in the new density region is computed (the particle is refracted), and the particle is retained at the boundary (or rather an infinitesimal distance beyond it in the new region) for the remainder of the current time interval.[42] In the next time interval, the calculation proceeds normally, with the particle starting out at this point near the boundary.

For the model with trapezoidal density distribution the refraction procedure is as follows. During a given time interval τ the particle is advanced in a straight line with a momentum corresponding to the potential-well depth at its position at the beginning of the time interval. At the end of the time interval τ the particle is refracted in accordance with the difference in well depths at the beginning and at the end of the interval. If the Monte Carlo procedure determines that an interaction has taken place in a given time interval, the procedure is the same as for a uniform-density model except, of course, that the new cascade particle must be refracted in the manner appropriate to the model that is used.

[42] It would, of course, be more correct to choose a new interaction partner in the new region, calculate the probability of interaction in the remaining time of the current interval, and let the particle advance the appropriate distance in the new region. However, the error introduced by our procedure is small.